nature photonics

ARTICLES

https://doi.org/10.1038/s41566-018-0123-6

Ultimate waveform reproducibility of extreme-ultraviolet pulses by high-harmonic generation in quartz

M. Garg, H. Y. Kim and E. Goulielmakis*

Optical waveforms of light reproducible with subcycle precision underlie applications of lasers in ultrafast spectroscopies, quantum control of matter and light-based signal processing. Nonlinear upconversion of optical pulses via high-harmonic generation in gas media extends these capabilities to the extreme ultraviolet (EUV). However, the waveform reproducibility of the generated EUV pulses in gases is inherently sensitive to intensity and phase fluctuations of the driving field. We used photoelectron interferometry to study the effects of intensity and carrier-envelope phase of an intense single-cycle optical pulse on the field waveform of EUV pulses generated in quartz nanofilms, and contrasted the results with those obtained in gas argon. The EUV waveforms generated in quartz were found to be virtually immune to the intensity and phase of the driving field, implying a non-recollisional character of the underlying emission mechanism. Waveform-sensitive photonic applications and precision measurements of fundamental processes in optics will benefit from these findings.

Waveform-reproducible intense pulses of light generated in the optical[1,2] and flanking spectral ranges[3,4] and their precise subcycle control underlie a wide range of spectacular developments in modern ultrafast science. Few-cycle[1] to single-cycle[4–6] or subcycle[2] optical pulses with a stabilized carrier-envelope phase (CEP) have made possible the steering of a wide range of atomic and molecular phenomena[7–9], the induction of petahertz currents in solids[10,11] and nanostructures[4,12] and the generation of the shortest impulses of soft X-rays[13–15].

Advancing attosecond precision measurement and control to their ultimate limits comes with the capability of generating waveform-reproducible probes in the extreme ultraviolet (EUV) and at multi-petahertz frequencies. This condition is primarily essential in experiments where the subtle changes in the temporal response of the system are encoded in the fine details of the structure of an attosecond probe waveform, such as the chirp, the duration and its timing to the driving field[16–18]. Failure to meet these conditions has been long identified as the source of noise in attosecond measurements[19,20]. The advancement of precision control of matter to the field cycle of multi-petahertz attosecond pulses further raises the above requirements and calls for control of EUV waveforms to be extended to their CEP[21].

The recollision picture as the dominant mechanism of EUV emission in atomic and molecular gases predicts that the phase of the emitted EUV light, Φ_{EUV}, strongly depends on the intensity of the driving field, I, as $\Delta\Phi_{\mathrm{EUV}}(I) \approx -\alpha\frac{I}{4\omega^3}$, where $\alpha(E)$ is the energy-dependent phase coefficient of the emission, which also depends on the atomic properties of the system, and ω is the carrier frequency of the driving optical pulses[22–24]. At the few-cycle and the single-cycle driving pulse limit where the intensity and CEP of an optical pulse are strongly coupled, the temporal structure of the EUV waveform turns extremely sensitive also to variation of the CEP of the generating field[13,25,26]. Whereas pulse intensity and CEP of an optical driver provide unique means for controlling the waveform of EUV radiation in gas high-harmonic emission[1,22,27], they also constitute hitherto imperfectly tamed sources of noise and compromise the reproducibility of the EUV waveform[19,20]. Ultimate limits of waveform synthesis and reproducibility in the EUV could be achieved if the generation mechanism was immune to intensity and CEP fluctuations of state-of-the-art driving laser sources. Here, we show that high-harmonic generation in bulk solids[3,28,29] and in particular in quartz[30,31] and the non-recollisional character of their emission mechanism allow this essential frontier in EUV photonics to be overcome.

Results

Driving-field intensity effects on the EUV waveform. High-harmonic generation from bulk solids[28] and their extension to mid-infrared[3,29] and EUV frequencies[30,31] has recently opened up new vistas in exploring new photonic regimes of solids under strong fields. The generation of high-harmonic field-reproducible waveforms from bulk solids has now been verified both in optical[3,32] and in EUV ranges[31]. Whereas the precise mechanism of high-harmonic emission in bulk solids is generally still debated[28–31,33,34], at least for quartz the evidence against a recollision picture—usually associated with the interband component of the polarization[35–38]—is steadily mounting[30,31,39,40].

To explore whether the non-recollision character of high harmonics in dielectrics can indeed provide an essential edge in producing waveform-reproducible EUV pulses, we used a photoemission-based interferometric[31,41] pulse phase measurement technique. In contrast to attosecond streaking[14,42], such an approach is sensitive to the CEP of the EUV pulse[41,43] and, as we show here, can provide detailed information on how the subcycle EUV waveform is modified against variation of the above parameters. In this approach, photoelectron spectra generated in a gas (see also Supplementary Section II) via its above-threshold ionization (ATI) by an optical pulse can be used as a reference to trace the phase of a broadband EUV pulse, which simultaneously ionizes the same medium. The critical information is encoded on the interference pattern and its variation against external parameters.

In our experiments, single-cycle pulses (precisely 1.2 cycles, carrier frequency $\omega_{\mathrm{L}} \approx 1.7$ eV, bandwidth $\Delta_{\mathrm{L}} \approx 1.1$–$3.1$ eV, duration

Max-Planck-Institut für Quantenoptik, Garching, Germany. *e-mail: elgo@mpq.mpg.de

© 2018 Macmillan Publishers Limited, part of Springer Nature. All rights reserved.

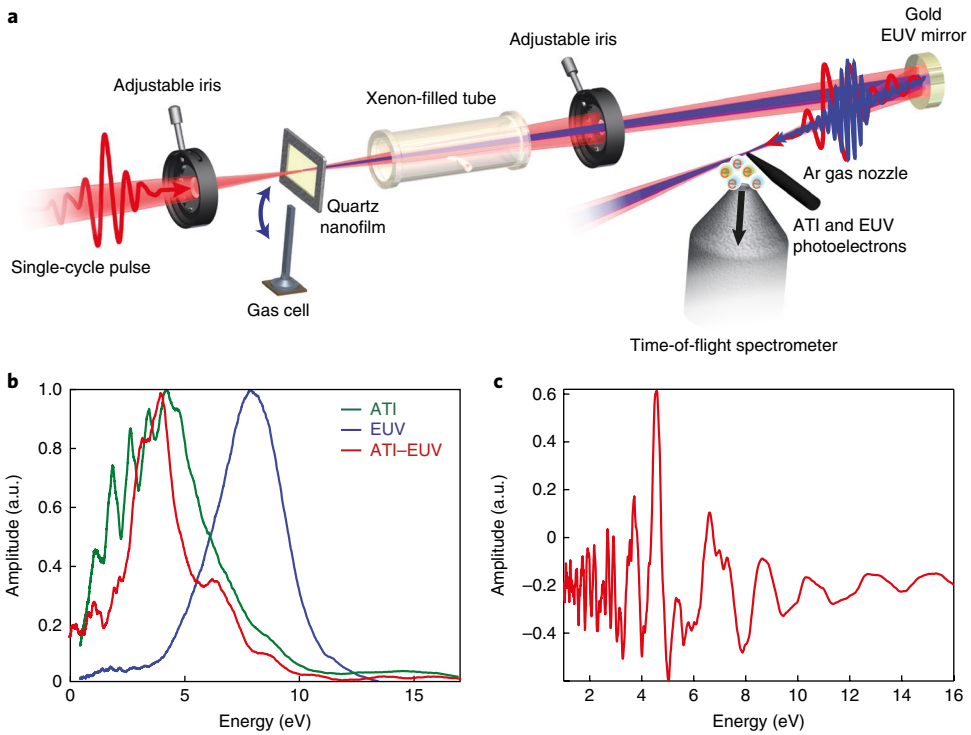

Fig. 1 | Photoelectron interferometric tracing of the phase of EUV pulses. a, Schematic diagram of the experimental set-up; quartz (~1 μm thick) or Ar gas jet are exposed to intense single-cycle optical pulses to generate coherent EUV emission. A time-of-flight spectrometer records electron spectra generated by EUV photoionization and ATI by optical pulses in Ar. Linear phase of EUV pulses can be controlled by varying the pressure in the xenon gas tube (see Supplementary Section V). **b**, ATI spectrum (green curve) generated by optical pulses, EUV photoelectron spectrum (blue curve) and their interference (red curve). **c**, Photoelectron interference pattern of ATI and EUV photoelectrons after background subtraction.

$\tau \approx 2.8$ fs, see also Supplementary Section I) generated in a light-field synthesizer[2] were focused either on a quasistatic gas cell filled with argon (Ar) or on a free-standing quartz nanofoil (thickness <1 μm) to generate EUV pulses (Fig. 1a). Quartz nanofoil was a *z*-cut single crystal with Γ–M direction in its Brillouin zone aligned along laser polarization to generate EUV radiation. The importance of keeping the sample as thin as possible, so as to avoid Kerr nonlinearities of the driving pulse before high-harmonic generation near the exit surface of the medium, is discussed in Supplementary Section IV. Moreover, the direct link between the formed interference fringes and the phase of the EUV pulse was verified by controlling the latter in a gas cell (see Supplementary Section V).

EUV and optical pulses were in turn focused by a single concave mirror onto an Ar jet placed under a time-of-flight electron spectrometer. Photoelectron spectra generated in Ar individually by direct EUV photoionization of Ar and ATI by the optical pulses are shown in Fig. 1b as blue and green lines, respectively. The conspicuous interference fringes emerging when both optical and EUV pulses interact with Ar are shown as a red curve in Fig. 1b. The subtraction of a static background from the red curve (ATI–EUV interference) in Fig. 1b, whose origin can be attributed to an imperfect spatial matching between EUV and ATI photoelectron beams at the detector[41], results in a robust and broadband (>10 eV) interference pattern (Fig. 1c). Interference fringe spacing of ~2.2 eV in Fig. 1c corresponds to a temporal separation of ATI- and EUV-generated electron pulses by ~1.8 fs, which is justified by the instantaneous photoionization by EUV and a rescattering time of ~1.8 fs for ATI electrons[41]. The observation of denser interference fringes (with spacing of ~0.3 eV) in the low energy part of the spectrum (Fig. 1c) is in accordance with simulations in earlier works[41].

In a first set of experiments, we kept the intensity of the optical pulse generating the ATI spectra in the second gas jet constant so as to provide a stable reference (see also Supplementary Fig. 2). We varied the intensity of the pulse, which drives EUV emission in Ar and quartz nonlinear media (Fig. 1a), and recorded photoelectron interference spectra as shown in Fig. 2a,b for Ar and quartz, respectively. In the case of Ar, the variation of the laser intensity is manifested as a prominent and energy-dependent shift of the interference pattern (Fig. 2a). In contrast, for quartz, the interference pattern remained robust over the entire range of intensities of the driving optical pulse (Fig. 2b). The maximum intensity in this case was constrained by the damage threshold of the quartz nanofilm to ~2.4×10^{13} W cm^{-2}. A detailed evaluation (see Supplementary Section II) of the CEP shift $\Delta\Phi_{\mathrm{CEP}}(I)$ and of the group delay dispersion (GDD) $\Delta\Phi''(I)$ variation at the carrier frequency of the EUV pulses for Ar (~34 eV) are shown by the red curves in Fig. 2c,d, and are contrasted with those of EUV pulses generated in quartz (central energy ~23 eV), shown by the blue lines in Fig. 2c,d, respectively.

Both $\Delta\Phi_{\mathrm{CEP}}(I)$ as well as the rapid variation of $\Delta\Phi''(I)$ in Ar as expressed also by evaluated slopes as $|\beta_{\mathrm{CEP}}| \approx 5 \times 10^{-2}\,\pi\,\mathrm{cm^2\,TW^{-1}}$ and $|\gamma_{\mathrm{GDD}}| \approx 32\,\mathrm{as^2\,cm^2\,TW^{-1}}$, respectively, are in excellent agreement with the findings of previous studies[24,44], as well as well-established semiclassical trajectory simulations[45] (see also Supplementary Section III) conducted here under the conditions of the experiments, shown by the red curves in Fig. 2e,f. The effects of the intensity on the generated EUV waveform are best visualized in Fig. 2g displaying the relative waveform (green and violet lines) variation for an intensity change of the driving pulses by ~5% as evaluated by the phase data of Fig. 2c,d. Other than the conspicuous change of the temporal profile, the waveform suffers a phase change greater than π rad, suggesting a very low level of reproducibility against intensity fluctuations.

By contrast, the phase properties of the EUV pulses emerging by the strong-field-driven quartz nanofilm exhibit a dramatically

© 2018 Macmillan Publishers Limited, part of Springer Nature. All rights reserved.

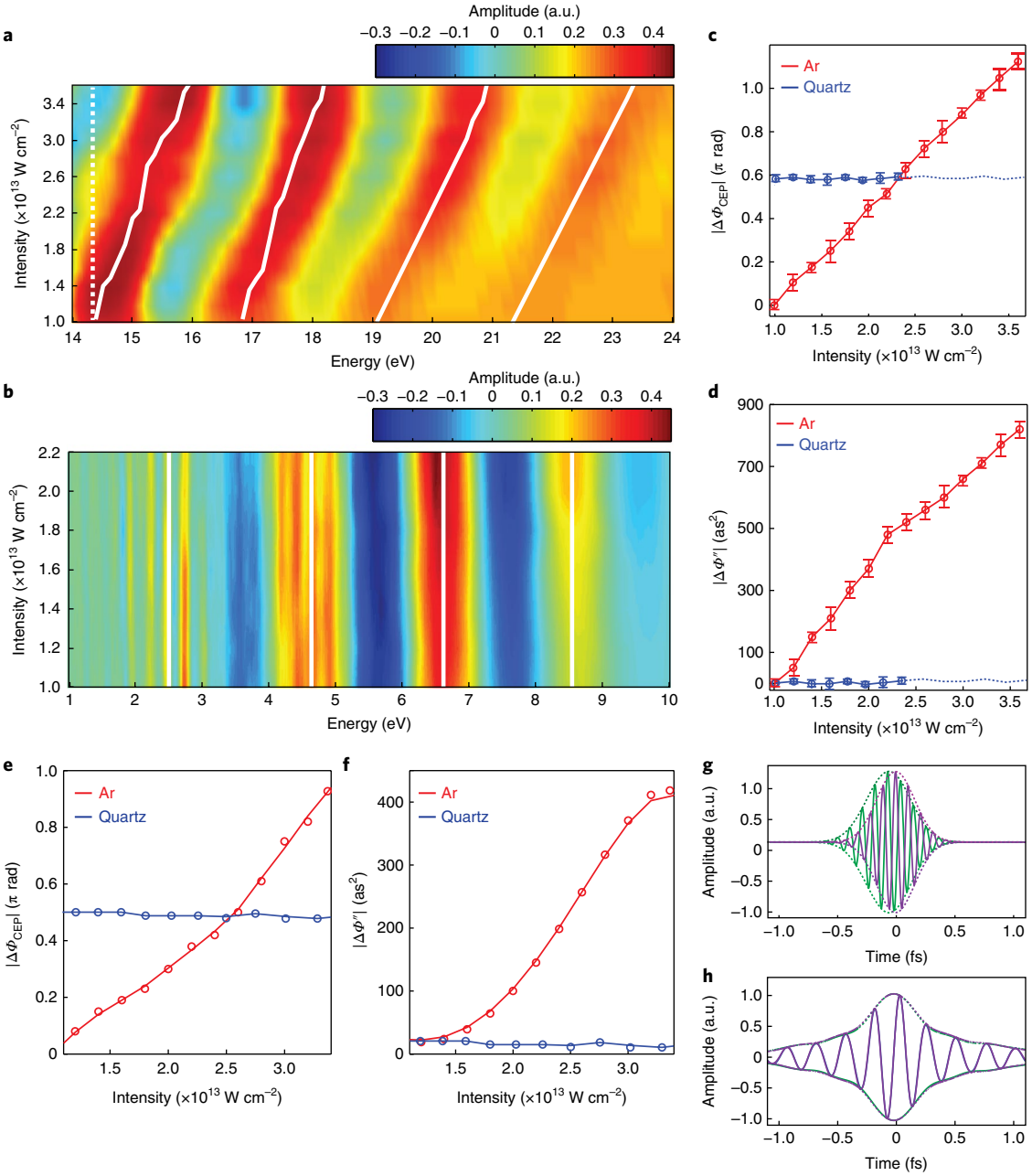

Fig. 2 | EUV waveform dependence on intensity of optical driver. a,**b**, Interference spectra of ATI and EUV photoelectrons recorded as a function of intensity of the driving laser pulse in Ar (**a**) and quartz (**b**) sources. White lines are a guide to the eye. **c**,**d**, Measured $\Delta\Phi_{CEP}$ (**c**) and $\Delta\Phi''$ (**d**) of EUV waveforms versus intensity of the driving pulse for Ar (red curve) and quartz (blue curve) sources. Error bars indicate standard error of the mean from three consecutive measurements. **e**,**f**, Simulated $\Delta\Phi_{CEP}$ (**e**) and $\Delta\Phi''$ (**f**) of EUV waveforms generated in Ar (red curve) and quartz (blue curve) as a function of the intensity of the driving laser pulse. **g**,**h**, Reconstructed (relative) EUV pulses for Ar (**g**) and quartz (**h**) for two different peak intensities of a single-cycle driver differing by 5%. The waveform in violet is taken as a reference and its phase is arbitrarily set to zero.

different dependence against the variations of the driving pulse intensity. The CEP shift $\Delta\Phi_{CEP}(I)$ (blue line, Fig. 2c) as well as the GDD variation (blue line, Fig. 2d) are both found to be negligible as also suggested by the evaluated slopes $|\beta_{CEP}| \approx 3\times10^{-4}\,\pi\,cm^2\,TW^{-1}$ and $|\gamma_{GDD}| \approx 5\times10^{-5}\,as^2\,cm^2\,TW^{-1}$, the lower margin of which is limited only by the accuracy of our experiments. These observations are not compatible with the nonlinearities of three-step model[46,47] in gases nor the generalized recollision picture[35] in solids, but can very well be reproduced by the intraband scattering picture[30,31,48] as suggested by the simulations (see also Supplementary Section III) of Fig. 2e,f (blue lines). In fact, theory predicts both slopes to be zero, that is, the EUV emission is immune to the variation of the intensity. These findings are better visualized in Fig. 2h (violet and green lines), where virtually identical and time-synchronous waveforms for the same intensity variation as in the gas phase simulation (Fig. 2g) (~5%) are evaluated from the sampled intensities in our interferometric measurements.

Driving-field CEP effects on the EUV waveform. In a second set of experiments, we investigated the robustness of the generated EUV waveforms in Ar gas and quartz nanofilms against the variation of the CEP of the driving optical pulses ($\Delta\eta_{Laser}$). Owing to our

© 2018 Macmillan Publishers Limited, part of Springer Nature. All rights reserved.

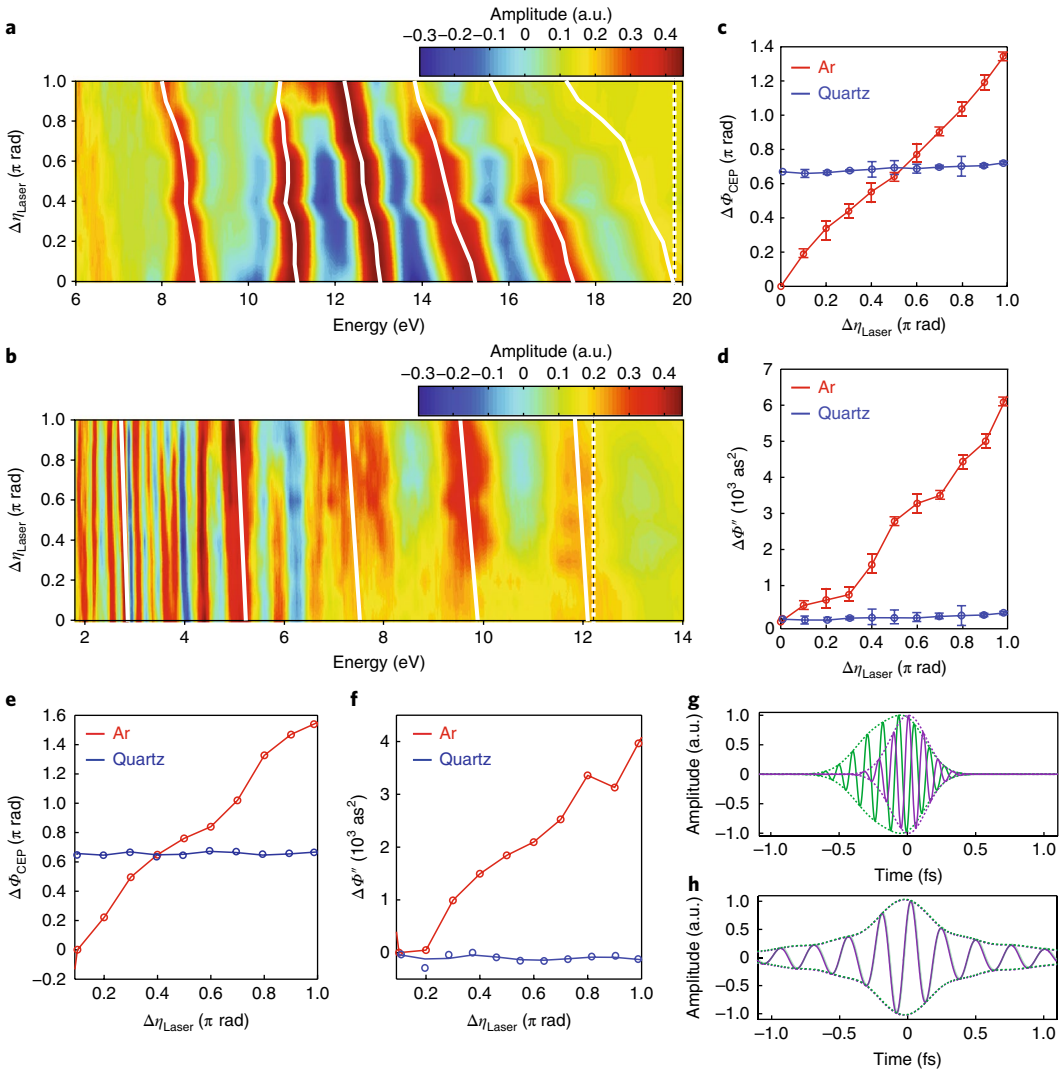

Fig. 3 | CEP effects of driving field on EUV waveform. a,**b**, Measured ATI–EUV interference spectra as a function of $\Delta\eta_{Laser}$ of driving laser pulse in Ar (**a**) and quartz (**b**). White lines are a guide to the eye. **c**,**d**, Measured $\Delta\Phi_{CEP}$ (**c**) and $\Delta\Phi''$ (**d**) of EUV pulses versus $\Delta\eta_{Laser}$ of the driving laser pulse for Ar (red curve) and quartz (blue curve). Error bars indicate standard error of the mean from three consecutive measurements. **e**,**f**, Simulated $\Delta\Phi_{CEP}$ (**e**) and $\Delta\Phi''$ (**f**) of EUV pulses in Ar (red curve) and quartz (blue curve) as a function of $\Delta\eta_{Laser}$ of the driving laser pulse. **g**,**h**, Reconstructed relative waveform variation of EUV pulses (shown as green and violet waveforms) for Ar (**g**) and quartz (**h**) for two different CEPs of a single-cycle driver differing by 0.2 π rad. The waveform in violet is taken as a reference and its phase is arbitrarily set to zero.

experimental geometry, we could not independently vary the CEP of driving pulses for EUV generation (first target, on the far left of Fig. 1a) and ATI generation (second gas jet in Fig. 1a). To overcome this constraint, we first characterized the phase variation $\Delta\chi_{ATI}$ of the ATI photoelectrons spectra as a function of the CEP of the driving field (see Supplementary Section II, Supplementary Figs. 6 and 7)[49]. In the next measurement, we traced the variation of the ATI–EUV photoelectron interference pattern as a function of CEP of the driving laser pulse, as is shown in Fig. 3a,b for Ar and quartz nanofilms, respectively. From the resulting phase curves, we subtract $\Delta\chi_{ATI}$ to obtain the pure phase variation of the EUV pulses $\Delta\Phi_{EUV}$ versus $\Delta\eta_{Laser}$ of the driving pulse for Ar and quartz.

Figure 3c,d contrasts the results of this study for Ar and quartz EUV nonlinear media. Although the variation of the CEP of the driving laser introduces a considerable shift in the CEP of the EUV pulse in the case of the Ar source (Fig. 3c, red line), the CEP of the EUV pulse emanating from quartz nanofilms remains virtually unaffected (Fig. 3c, blue line). Similar conclusions can be obtained by evaluating the variation of the $\Delta\Phi''$ of EUV pulses for both cases, as shown in Fig. 3d, red and blue lines for Ar and quartz, respectively. Slopes of variation of $\Delta\Phi_{CEP}$ and $\Delta\Phi''$ for Ar are $\varepsilon_{CEP} = 1.4$ and $\delta_{GDD} \approx 6{,}200\,as^2\pi^{-1}$, respectively, which are nearly zero for quartz. The results of semiclassical trajectory calculations[45] in Fig. 3e,f (red lines) confirm once again the compatibility of our findings in Ar with the recollision picture. Similarly, as in the previous study, we evaluate the relative variation of the EUV waveforms in the time domain for a shift of $\Delta\eta_{Laser} = 0.2\pi$ rad of the driving single-cycle pulse for Ar in Fig. 3g and quartz in Fig. 3h.

In the case of Ar, the emerging EUV pulses do not maintain any of their key properties such as their CEP, the temporal profile (chirp) or their timing relative to the driving field (Fig. 3g). The EUV waveform undergoes a dramatic distortion on variation of CEP of the driver pulse, which is manifested by an apparent phase shift of the carrier wave and doubling of the waveform duration. By contrast, and in close agreement with the predictions of the intraband scattering model, the waveforms of the EUV pulses (Fig. 3h) emerging from quartz perfectly preserve their precise temporal structure as well as the timing to the driving field.

© 2018 Macmillan Publishers Limited, part of Springer Nature. All rights reserved.

Our results allow the question to be answered: what are the margins of intensity and phase noise of ultrafast intense laser pulses so that they assure reproducibility of EUV waveforms in gas phase high-harmonic generation at precision similar to that attained for intense pulses in the optical regime[50], that is, of the order of ~π/20 of their field waveform? Our data in Figs. 2 and 3 and their evaluation allow us to estimate that a pulse-to-pulse intensity stability of ~0.25% and a waveform reproducibility better than ~π/100 of the optical field cycle would be required for the driving optical pulse. These requirements are beyond the reach of contemporary high-power few-cycle pulse technology. By contrast, the immunity of EUV waveform generated in quartz to intensity and phase fluctuations of the driver demonstrated here allows us to overcome directly this frontier with existing intense pulse technologies.

Strong-field-driven dielectrics generate multi-petahertz pulses of light of unprecedented waveform robustness against intensity and CEP variation of the driving source and surpass this of noble gases by many orders of magnitude. Our experiments suggest that the immunity of the generated EUV waveforms to these parameters can be attributed to the fundamentally different, non-recollisional character of the high-harmonic emission in bulk quartz. Our approach can be extended to explore the physics of high-harmonic generation at lower energies, for example in semiconductors. In this case, the gas-based ATI electrons could be replaced by ATI electrons from metal nanotips[51–53], taking advantage of the low work function (~5 eV) and the established similarity of strong-field ionization in atoms and metals. We anticipate that high-harmonic EUV waveforms immune to intensity and CEP fluctuations of the driving source will also substantially contribute towards exploring new frontiers in technologies such as EUV frequency combs.

Data availability. The data that support the plots within this paper and other findings of this study are available from the corresponding author upon reasonable request.

Received: 4 November 2017; Accepted: 6 February 2018;
Published online: 12 March 2018

References

1. Baltuska, A. et al. Attosecond control of electronic processes by intense light fields. *Nature* **421**, 611–615 (2003).
2. Hassan, M. T. et al. Optical attosecond pulses and tracking the nonlinear response of bound electrons. *Nature* **530**, 66–70 (2015).
3. Schubert, O. et al. Sub-cycle control of terahertz high-harmonic generation by dynamical Bloch oscillations. *Nat. Photon.* **8**, 119–123 (2014).
4. Rybka, T. et al. Sub-cycle optical phase control of nanotunnelling in the single-electron regime. *Nat. Photon.* **10**, 667–670 (2016).
5. Wirth, A. et al. Synthesized light transients. *Science* **334**, 195–200 (2011).
6. Huang, S. W. et al. High-energy pulse synthesis with sub-cycle waveform control for strong-field physics. *Nat. Photon.* **5**, 475–479 (2011).
7. Sansone, G. et al. Electron localization following attosecond molecular photoionization. *Nature* **465**, 763–766 (2010).
8. Kling, M. F. et al. Control of electron localization in molecular dissociation. *Science* **312**, 246–248 (2006).
9. Huismans, Y. et al. Time-resolved holography with photoelectrons. *Science* **331**, 61–64 (2011).
10. Schiffrin, A. et al. Optical-field-induced current in dielectrics. *Nature* **493**, 70–74 (2013).
11. Higuchi, T., Heide, C., Ullmann, K., Weber, H. B. & Hommelhoff, P. Light-field-driven currents in graphene. *Nature* **550**, 224–228 (2017).
12. Sivis, M. et al. Tailored semiconductors for high-harmonic optoelectronics. *Science* **357**, 303–306 (2017).
13. Goulielmakis, E. et al. Single-cycle nonlinear optics. *Science* **320**, 1614–1617 (2008).
14. Sansone, G. et al. Isolated single-cycle attosecond pulses. *Science* **314**, 443–446 (2006).
15. Li, J. et al. 53-attosecond X-ray pulses reach the carbon K-edge. *Nat. Commun.* **8**, 186 (2017).
16. Cavalieri, A. L. et al. Attosecond spectroscopy in condensed matter. *Nature* **449**, 1029–1032 (2007).
17. Schultze, M. et al. Delay in photoemission. *Science* **328**, 1658–1662 (2010).
18. Guenot, D. et al. Measurements of relative photoemission time delays in noble gas atoms. *J. Phys. B* **47**, 245602 (2014).
19. Wang, H. et al. Practical issues of retrieving isolated attosecond pulses. *J. Phys. B* **42**, 134007 (2009).
20. Gagnon, J. & Yakovlev, V. S. The robustness of attosecond streaking measurements. *Opt. Express* **17**, 17678–17693 (2009).
21. Peng, L. Y. & Starace, A. F. Attosecond pulse carrier-envelope phase effects on ionized electron momentum and energy distributions. *Phys. Rev. A* **76**, 043401 (2007).
22. Lewenstein, M., Salières, P. & L'Huillier, A. Phase of the atomic polarization in high-order harmonic generation. *Phys. Rev. A* **52**, 4747–4754 (1995).
23. Yost, D. C. et al. Vacuum-ultraviolet frequency combs from below-threshold harmonics. *Nat. Phys.* **5**, 815–820 (2009).
24. Corsi, C., Pirri, A., Sali, E., Tortora, A. & Bellini, M. Direct interferometric measurement of the atomic dipole phase in high-order harmonic generation. *Phys. Rev. Lett.* **97**, 023901 (2006).
25. Sansone, G. et al. Measurement of harmonic phase differences by interference of attosecond light pulses. *Phys. Rev. Lett.* **94**, 193903 (2005).
26. Sansone, G. et al. Observation of carrier-envelope phase phenomena in the multi-optical-cycle regime. *Phys. Rev. Lett.* **92**, 113904 (2004).
27. Haworth, C. A. et al. Half-cycle cutoffs in harmonic spectra and robust carrier-envelope phase retrieval. *Nat. Phys.* **3**, 52–57 (2007).
28. Ghimire, S. et al. Observation of high-order harmonic generation in a bulk crystal. *Nat. Phys.* **7**, 138–141 (2011).
29. Vampa, G. et al. Linking high harmonics from gases and solids. *Nature* **522**, 462–464 (2015).
30. Luu, T. T. et al. Extreme ultraviolet high-harmonic spectroscopy of solids. *Nature* **521**, 498–502 (2015).
31. Garg, M. et al. Multi-petahertz electronic metrology. *Nature* **538**, 359–363 (2016).
32. Langer, F. et al. Symmetry-controlled temporal structure of high-harmonic carrier fields from a bulk crystal. *Nat. Photon.* **11**, 227–231 (2017).
33. Hohenleutner, M. et al. Real-time observation of interfering crystal electrons in high-harmonic generation. *Nature* **523**, 572–575 (2015).
34. Higuchi, T., Stockman, M. I. & Hommelhoff, P. Strong-field perspective on high-harmonic radiation from bulk solids. *Phys. Rev. Lett.* **113**, 213901 (2014).
35. Vampa, G. et al. Theoretical analysis of high-harmonic generation in solids. *Phys. Rev. Lett.* **113**, 073901 (2014).
36. Golde, D., Meier, T. & Koch, S. W. High harmonics generated in semiconductor nanostructures by the coupled dynamics of optical inter- and intraband excitations. *Phys. Rev. B* **77**, 075330 (2008).
37. Golde, D., Meier, T. & Koch, S. W. Microscopic analysis of extreme nonlinear optics in semiconductor nanostructures. *J. Opt. Soc. Am. B* **23**, 2559–2565 (2006).
38. You, Y. S. et al. Laser waveform control of extreme ultraviolet high harmonics from solids. *Opt. Lett.* **42**, 1816–1819 (2017).
39. Hammond, T. J. et al. Integrating solids and gases for attosecond pulse generation. *Nat. Photon.* **11**, 594–599 (2017).
40. You, Y. S. et al. High-harmonic generation in amorphous solids. *Nat. Commun.* **8**, 724 (2017).
41. Liu, C. D. et al. Carrier-envelope phase effects of a single attosecond pulse in two-color photoionization. *Phys. Rev. Lett.* **111**, 123901 (2013).
42. Goulielmakis, E. et al. Direct measurement of light waves. *Science* **305**, 1267–1269 (2004).
43. He, P. L., Ruiz, C. & He, F. Carrier-envelope-phase characterization for an isolated attosecond pulse by angular streaking. *Phys. Rev. Lett.* **116**, 203601 (2016).
44. Benko, C. et al. Extreme ultraviolet radiation with coherence time greater than 1 s. *Nat. Photon.* **8**, 530–536 (2014).
45. Lewenstein, M., Balcou, P., Ivanov, M. Y., L'Huillier, A. & Corkum, P. B. Theory of high-harmonic generation by low-frequency laser fields. *Phys. Rev. A* **49**, 2117–2132 (1994).
46. Corkum, P. B. Plasma perspective on strong-field multiphoton ionization. *Phys. Rev. Lett.* **71**, 1994–1997 (1993).
47. Schafer, K. J., Yang, B., Dimauro, L. F. & Kulander, K. C. Above threshold ionization beyond the high harmonic cutoff. *Phys. Rev. Lett.* **70**, 1599–1602 (1993).
48. Wu, M. X., Ghimire, S., Reis, D. A., Schafer, K. J. & Gaarde, M. B. High-harmonic generation from Bloch electrons in solids. *Phys. Rev. A* **91**, 043839 (2015).
49. Ott, C. et al. Strong-field spectral interferometry using the carrier-envelope phase. *New J. Phys.* **15**, 073031 (2013).

© 2018 Macmillan Publishers Limited, part of Springer Nature. All rights reserved.

50. Fordell, T., Miranda, M., Arnold, C. L. & L'Huillier, A. High-speed carrier-envelope phase drift detection of amplified laser pulses. *Opt. Express* **19**, 23652–23657 (2011).
51. Kruger, M., Schenk, M. & Hommelhoff, P. Attosecond control of electrons emitted from a nanoscale metal tip. *Nature* **475**, 78–81 (2011).
52. Herink, G., Solli, D. R., Gulde, M. & Ropers, C. Field-driven photoemission from nanostructures quenches the quiver motion. *Nature* **483**, 190–193 (2012).
53. Piglosiewicz, B. et al. Carrier-envelope phase effects on the strong-field photoemission of electrons from metallic nanostructures. *Nat. Photon.* **8**, 37–42 (2014).

Acknowledgements

We thank D. Bauer and C. Gohle for discussions. This work was supported by the Max Planck Society, a European Research Council grant (Attoelectronics-258501), the Deutsche Forschungsgemeinschaft, the Cluster of Excellence, Munich Centre for Advanced Photonics, and the European Research Training Network (MEDEA-641789).

Author contributions

M.G. and H.Y.K. conducted the experiments; M.G. and E.G. conceived the experiments. E.G. planned the experiments and supervised the project; all authors interpreted data and contributed to the preparation of the manuscript.

Competing interests

The authors declare no competing interests.

Additional information

Supplementary information is available for this paper at https://doi.org/10.1038/s41566-018-0123-6.

Reprints and permissions information is available at www.nature.com/reprints.

Correspondence and requests for materials should be addressed to E.G.

Publisher's note: Springer Nature remains neutral with regard to jurisdictional claims in published maps and institutional affiliations.

© 2018 Macmillan Publishers Limited, part of Springer Nature. All rights reserved.